JOURNAL OF THERMOPHYSICS AND HEAT TRANSFER
Vol. 14, No. 3, July–September 2000

Analysis of Transient Conjugate Heat Transfer to a Free Impinging Jet

Muhammad M. Rahman* and Antonio J. Bula†
University of South Florida, Tampa, Florida 33620-5350
and
John E. Leland‡
U.S. Air Force Research Laboratory, Wright–Patterson Air Force Base, Ohio 45433-7251

Transient conjugate heat transfer during the impingement of a freejet of high Prandtl number fluid on a solid disk of finite thickness is considered. When power is turned on at $t = 0$, a uniform heat flux is imposed on the disk surface. The numerical model considers both solid and fluid regions. Equations for the conservation of mass, momentum, and energy are solved in the liquid region, with the transport processes at the inlet and exit boundaries, as well as at the solid–liquid and liquid–gas interfaces taken into account. In the solid region, only heat conduction equation is solved. The shape and location of the free surface (liquid–gas interface) is determined iteratively as a part of the solution process by satisfying the kinematic condition as well as the balance of normal and shear forces at this interface. Computed results include the velocity, temperature, and pressure distributions in the fluid and the local and average heat transfer coefficients at the solid–fluid interface. Computations are carried out to investigate the influence of different operating parameters such as jet velocity, disk thickness, and disk material.

Nomenclature

b = thickness of the disk, m
c_p = specific heat at constant pressure, kJ/kg · K
d_n = diameter of the nozzle, m
Fo = Fourier number, $\alpha_f t / d_n^2$
g = acceleration due to gravity, m/s^2
H_n = distance of the nozzle from the disk, m
h = heat transfer coefficient, $q_{\text{int}}/(T_{\text{int}} - T_j)$, W/m^2 · K
h_{av} = heat transfer coefficient, W/m^2 · K:

$$\frac{2}{r_0^2(\bar{T}_{\text{int}} - T_j)} \int_0^{r_0} hr(T_{\text{int}} - T_j)\, \mathrm{d}r$$

k = thermal conductivity, W/m · K
Nu = Nusselt number, hr/k_f
Nu_{av} = average Nusselt number, $h_{\text{av}} r_0 / k_f$
n = coordinate normal to the free surface, m
p = pressure, Pa
q = heat flux, W/m^2
$\bar{q}$ = average heat flux, W/m^2
Re = Reynolds number, $\rho_f v_j d_n / \mu$
r = radial coordinate, m
r_n = radius of the nozzle, m
r_0 = Radius of the disk, m
T = temperature, K
$\bar{T}_{\text{int}}$ = average interface temperature, K:

$$\frac{2}{r_0^2} \int_0^{r_0} T_{\text{int}}\, r\, \mathrm{d}r$$

T_j = jet temperature, K
t = time, s
v_i = initial velocity field, m/s
v_j = jet velocity, m/s
v_r = radial velocity, m/s
v_t = velocity along the free surface, m/s
v_z = axial velocity, m/s
z = axial coordinate, m
α = thermal diffusivity, m^2/s
δ = height of the free surface from the disk, m
θ = dimensionless temperature, $(T - T_j)/(q_w d_n / k_f)$, K
μ = dynamic viscosity of the fluid, kg/m · s
ρ = density, kg/m^3
σ = surface tension coefficient, N/m

Subscripts

atm = atmospheric condition
av = average
f = fluid
int = solid–fluid interface
s = solid
w = bottom surface of the disk

Received 23 February 1999; revision received 1 March 2000; accepted for publication 2 March 2000.

*Associate Professor, Department of Mechanical Engineering.
†Research Assistant, Department of Mechanical Engineering; currently Assistant Professor, Departamento de Ingenieria Mecanica, Universidad Del Norte, Km 5 Carretera Puerto Colombia, Barranquilla, Colombia.
‡Research Engineer, Aero Propulsion and Power Directorate.

Introduction

JET impingement heat transfer is known for its ease of implementation and high heat transfer coefficients. It has been employed for the drying of paper and textiles, tempering glass, bearing cooling, turbine blade cooling, and electronics cooling. Although a poor heat transfer fluid, lubricating oil is an attractive coolant for aircraft applications because it is generally in close proximity to the electrical generating equipment. It is also preexisting in the aircraft and, therefore, does not require flight qualification, new maintenance procedures, additional inventory space and logistics procedures, or additional environmental protection guidelines. These advantages translate into greatly reduced operational costs, which may far overweigh the loss in cooling efficiency. Lubricating oils are generally known for their large Prandtl number and strong dependence of viscosity on temperature. Alternately, air cooling is generally inadequate or undesirable because of the additional drag imposed by ram air heat exchangers. Therefore, the investigation of jet impingement heat transfer for high Prandtl number fluids taking into account the effects of property variation with temperature is of great importance to the military and the commercial aircraft industry.

Free-surface jets are formed when a liquid issues from a nozzle or orifice into a gaseous environment. The free surface forms immediately at the nozzle exit and prevails through the impingement

region and into the wall jet region. The shape of the free surface depends on gravitational, surface tension, and pressure forces. The jet speed, size, and orientation determine the magnitude of these forces. In the past, several studies have been carried out on heat transfer during freejet impingement. Glauert[1] considered the flow due to a jet spreading out over a plane surface, either radially or in two dimensions. Solutions to the boundary-layer equations were sought, according to which the form of the velocity distribution across the jet did not vary along its length.

Metzger et al.[2] presented results for heat transfer characteristics of a circular liquid jet impinging normally on a plane surface. The experimental procedure was developed to cover jets formed by water or synthetic-base lubricating oil and included a significant Prandtl number range so that extension to other liquids could be made. Hrycak[3] carried out an investigation of heat transfer from a round jet impinging normally on a flat plate. This study was done for various nozzle-to-target distances, with Reynolds number varying from 1.4×10^4 to 6.7×10^4, and for different nozzle diameters. Liu and Lienhard[4] investigated a circular subcooled liquid jet impinging on a surface maintained at a uniform heat flux. They used an integral method to obtain analytical predictions of temperature distribution in the liquid film and the local Nusselt number. They also carried out experiments to test the predictions of the theory.

Wang et al.[5–7] presented an analytical study of heat transfer between an axisymmetric free impinging jet and a solid flat disk with a nonuniform wall temperature or wall heat flux. Stevens and Webb[8] carried out an experimental investigation to characterize local heat transfer coefficient for a round, free liquid jet impinging normally over a flat uniform heat flux surface. Liu et al.[9] presented an analytical and experimental investigation for jet impingement cooling of uniformly heated surfaces to determine local Nusselt numbers from the stagnation point to radii up to 40 diameters. Womac et al.[10] obtained experimental data for liquid jet impingement cooling of small square heat sources resembling integrated circuit chips. Both free-surface and submerged jet configurations were studied for a range of velocities, nozzle diameters, and nozzle-to-heater distances. Two different liquids, water and FC-77, were used as coolants. Elison and Webb[11] studied transport from a small-diameter, fully developed liquid jet impinging normally over a constant heat flux surface. Alkam and Butler[12] applied an explicit finite difference technique to solve the case of transient, forced convective conjugate heat transfer between an axisymmetric incompressible laminar impinging jet and a solid disk at the stagnation zone. Constant properties were considered, and no viscous dissipation was taken into account.

Ma et al.[13–15] performed an experimental study to investigate the local convective heat transfer from a vertical heated surface to an obliquely impinging circular free-surface jet of transformer oil. Lee et al.[16] conducted a numerical study to characterize the thermal behavior of laminar circular liquid jets. The effects of different parameters investigated included Reynolds number, Prandtl number, nozzle-to-disk distance, jet velocity, nozzle diameter, and velocity profile at the nozzle exit. Leland and Pais[17] performed an experimental investigation to determine the heat transfer rate for an impinging free-surface axisymmetric jet of lubricating oil for a wide range of Prandtl numbers and for conditions varying inside the fluid film. They concluded that the heat transfer surface configuration has an important effect on the Nusselt number. The effect of recovery temperature could be correlated by $Pr^{0.47}$. For constant flow rate or Reynolds number, larger nozzle diameters were shown to give higher heat transfer rates.

Even though there has been an impressive amount of research work on freejet impingement, there has been no attempt to model numerically the conjugate heat transfer process where heat is transmitted through a solid body from a heat source located on one side and where fluid is impinging on the opposite side. In addition, the variation of fluid properties with temperature has not been taken into account in any previous numerical work and has been assumed to be negligible in most analytical work. When the lubricating oil is used as the coolant and temperature difference between the jet and the disk is large, the property variation within the flowfield can greatly affect the heat transfer process. In addition, transient heat transfer has been considered only in the study of Alkam and Butler.[12] The results of this study are applicable only in the stagnation zone and limited to negligible property variations. Therefore, the development of a numerical model for transient conjugate heat transfer during freejet impingement, taking into account the variation of fluid properties with location and time, is expected to be a very valuable contribution to the state of the art of jet impingement cooling system design for aircraft applications.

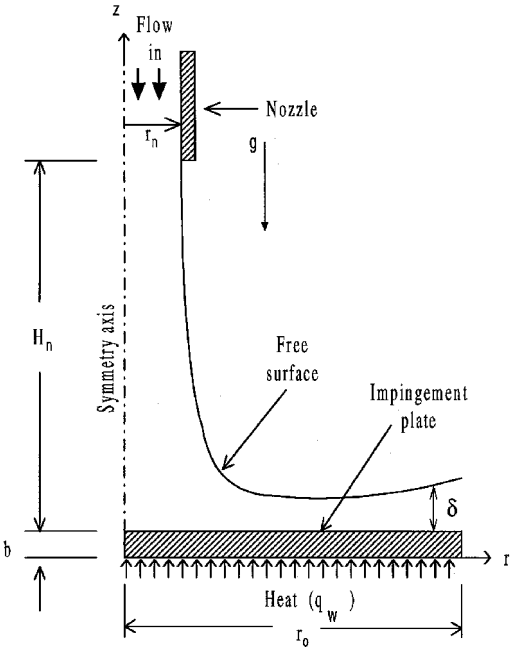

Fig. 1 Axial jet impingement.

Mathematical Model

Consider an axial jet discharging from a circular nozzle and impinging on a uniformly heated solid disk as shown in Fig. 1. The power is turned on and the heat source starts supplying the heat after an isothermal steady-state flow field has been established on the disk. When the fluid is considered to be incompressible with properties dependent on temperature only, the equations describing the conservation of mass, momentum, and energy in cylindrical coordinates can be written as (Ref. 18)

$$\frac{1}{r}\frac{\partial}{\partial r}(\rho_f r v_r) + \frac{\partial}{\partial z}(\rho_f v_z) = 0 \tag{1}$$

$$\rho_f\left(\frac{\partial v_r}{\partial t} + v_r\frac{\partial v_r}{\partial r} + v_z\frac{\partial v_r}{\partial z}\right) = -\frac{\partial p}{\partial r} + \frac{1}{r}\frac{\partial}{\partial r}\left(\frac{2}{3}r\mu\left(2\frac{\partial v_r}{\partial r} - \frac{v_r}{r} - \frac{\partial v_z}{\partial z}\right)\right) + \frac{\partial}{\partial z}\left(\mu\left(\frac{\partial v_r}{\partial z} + \frac{\partial v_z}{\partial r}\right)\right) \tag{2}$$

$$\rho_f\left(\frac{\partial v_z}{\partial t} + v_r\frac{\partial v_z}{\partial r} + v_z\frac{\partial v_z}{\partial z}\right) = -\rho_f g - \frac{\partial p}{\partial z} + \frac{1}{r}\frac{\partial}{\partial r}\left(r\mu\left(\frac{\partial v_r}{\partial z} + \frac{\partial v_z}{\partial r}\right)\right) + \frac{\partial}{\partial z}\left(\frac{2}{3}\mu\left(2\frac{\partial v_z}{\partial z} - \frac{v_r}{r} - \frac{\partial v_r}{\partial r}\right)\right) \tag{3}$$

$$\rho_f\left[\frac{\partial\left(c_{p_f}T_f\right)}{\partial t}+v_r\frac{\partial\left(c_{p_f}T_f\right)}{\partial r}+v_z\frac{\partial\left(c_{p_f}T_f\right)}{\partial z}\right]$$
$$=\left(\frac{1}{r}\frac{\partial}{\partial r}\left(rk_f\frac{\partial T_f}{\partial r}\right)+\frac{\partial}{\partial z}\left(k_f\frac{\partial T_f}{\partial z}\right)\right)+\left(v_z\frac{\partial p}{\partial z}+v_r\frac{\partial p}{\partial r}\right)$$
$$+\mu_f\left\{2\left[\left(\frac{\partial v_r}{\partial r}\right)^2+\left(\frac{v_r}{r}\right)^2+\left(\frac{\partial v_z}{\partial z}\right)^2\right]\right.$$
$$\left.+\left(\frac{\partial v_r}{\partial z}+\frac{\partial v_z}{\partial r}\right)^2-\frac{2}{3}\left(\frac{\partial v_r}{\partial r}+\frac{v_r}{r}+\frac{\partial v_z}{\partial z}\right)^2\right\} \quad (4)$$

The variation of thermal conductivity within the solid was found to be significant for some materials such as diamond. Therefore, considering variable properties, the equation describing the conservation of energy can be written as follows:

$$\frac{1}{r}\frac{\partial}{\partial r}\left(rk_s\frac{\partial T_s}{\partial r}\right)+\frac{\partial}{\partial z}\left(k_s\frac{\partial T_s}{\partial z}\right)=\rho_s c_{p_s}\frac{\partial T_s}{\partial t} \quad (5)$$

Equations (1–5) are subjected to the following boundary conditions. At $r=0$, $0\le z\le b$:

$$\frac{\partial T_s}{\partial r}=0 \quad (6)$$

At $r=0$, $b\le z\le H_n$:

$$v_r=0,\qquad \frac{\partial v_z}{\partial r}=0,\qquad \frac{\partial T_f}{\partial r}=0 \quad (7)$$

At $r=r_0$, $0\le z\le b$:

$$\frac{\partial T_s}{\partial r}=0 \quad (8)$$

At $r=r_0$, $b\le z\le\delta$:

$$p=p_{\text{atm}} \quad (9)$$

At $z=0$:

$$-k_s\frac{\partial T_s}{\partial z}=q_w \quad (10)$$

At $z=b$:

$$T_s=T_f,\qquad v_r=0,\qquad v_z=0,\qquad k_s\frac{\partial T_s}{\partial z}=k_f\frac{\partial T_s}{\partial z} \quad (11)$$

At $z=b+H_n$, $0\le r\le r_n$:

$$v_r=0,\qquad v_z=-v_j,\qquad T_f=T_j \quad (12)$$

Note that the outer edge of the disk has been assumed to be insulated. The fluid at $r=r_0$ was assumed to have negligible conduction in the radial direction ($\partial T_f/\partial_r=0$) leaving only convective outflow at that location. At the free surface, the boundary conditions can be expressed as follows. At $z=\delta$, $r_n<r<r_0$:

$$\frac{\mathrm{d}\delta}{\mathrm{d}r}=\frac{v_z}{v_r},\qquad p=p_{\text{atm}}-\sigma\frac{\mathrm{d}^2\delta}{\mathrm{d}r^2}\Bigg/\left[1+\left(\frac{\mathrm{d}\delta}{\mathrm{d}r}\right)^2\right]^{\frac{3}{2}}$$
$$\frac{\partial v_t}{\partial n}=0,\qquad \frac{\partial T_f}{\partial n}=0 \quad (13)$$

Equations (13) essentially indicate the kinematic condition, balance of normal forces, balance of shear forces, and adiabatic condition at the free surface. These equations were derived from more general equations presented by White.[19] Note that n indicates direction normal to the free surface. The frictional resistance and heat transfer to the surrounding gaseous medium has been assumed to be negligible. The viscous normal stresses have been neglected in the balance of normal forces. The negligible heat transfer from the free surface to the surrounding gaseous medium, including the effects of radiation and evaporation is quite appropriate for a moderate rate of heat transfer from the disk to the thin liquid film.[20] The model has to be modified for higher rate of heat transfer that results in evaporation at the free surface by taking into account the latent heat of evaporation.

The disk and the fluid were assumed to be in an equilibrium isothermal condition at the start of the transient heating process. This is expressed as follows. At $t=0$:

$$T_s=T_f=T_j,\qquad v=v_i(r,z) \quad (14)$$

Note that the preceding mathematical model is based on the assumption of two-dimensional axisymmetric flow and heat transfer. In practice, such free-surface liquid flows are often three dimensional, despite the two dimensionality of the jet generation apparatus. The secondary flows are results of vortices that develop on stagnation in the flow, and whose axes extend radially outward from the stagnation point.

Numerical Computation

The governing equations along with the boundary conditions described in the preceding section were solved using the finite element method. The computation domain was divided into a number of quadrilateral elements. The dependent variables (i.e., velocity, pressure, and temperature) were interpolated to a set of nodal points that defined the elements. In each element, the velocity, pressure, and temperature fields were approximated, which led to a set of equations that defined the continuum. To solve the position of the free surface, a new degree of freedom at the nodes on the free surface was introduced into the global system of equations. The discretization of governing transport equations and boundary conditions was carried out using the Galerkin formulation. The solution of the resulting algebraic equations was carried out using the Newton–Raphson method. Because the solution of the momentum equation required only two out of the three boundary conditions at the free surface, the third condition was used to upgrade the position of the free surface at the end of each iteration step.

To determine the initial velocity field, $v_i(r,z)$, equations for the conservation of mass and momentum were solved. Once the initial free-surface height distribution and the flowfield for an isothermal equilibrium condition was established, the power at the heat source was turned on. The computation domain covered both solid and fluid regions, and equations for the conservation of mass, momentum, and energy were solved simultaneously as a conjugate problem taking into account the variation of fluid and solid properties with temperature. At each time step, the solution was considered converged when the field values did not change from one iteration to the next, and the sum of residuals for each degree of freedom was less than $1E$-08. Computation was continued marching forward with time until a steady-state condition was reached. Because of large changes at the outset of the transient and very small changes when the solution approached the steady-state condition, a variable time step was used for the computation.

Results and Discussion

The simulation was carried out for three different materials, namely, copper, diamond, and constantan. The working fluid used for the simulation was Mil-7808, which is a lubricating oil used in aircrafts. The relevant fluid properties were calculated from the following correlating equations, which are valid for $303<T_f<390$ K: $c_{pf}=903.8+3.332T_f$, $k_f=0.18-1\times10^{-4}T_f$, $\rho_f=1181-0.708T_f$, and $\mu=0.941-5.07\times10^{-3}T_f+6.87\times10^{-6}T_f^2$. The range of Prandtl number encountered in the present investigation was 169–384. The distance of the nozzle from the disk ($H_n=0.0085$ m), diameter of the nozzle ($d_n=0.0017$ m), and radius of the disk ($r_0=0.0065$ m) were kept constant during the simulation.

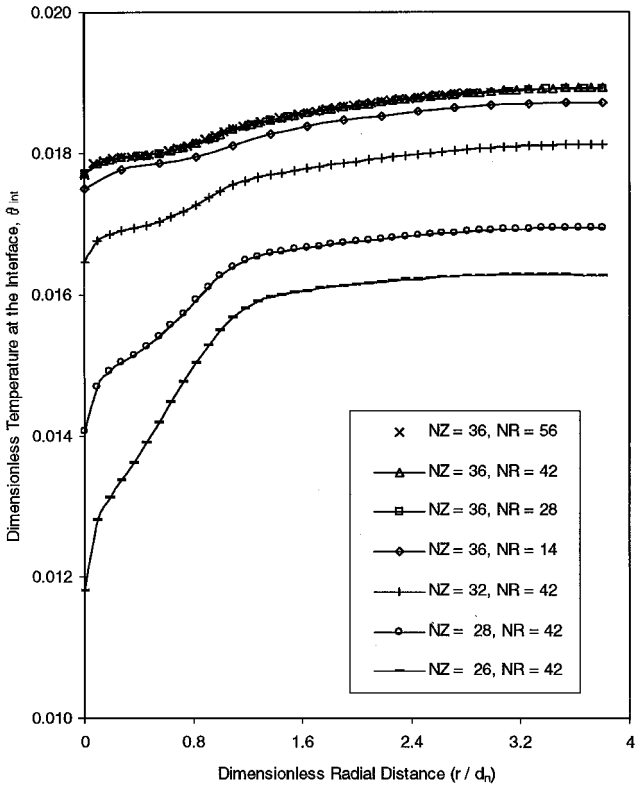

Fig. 2 Dimensionless temperature at the interface for different number of elements in axial and radial directions ($Re = 1100$, $T_j = 348$ K, $b/d_n = 2.94$, $H_n/d_n = 5$, copper plate, and $q_w = 63$ kW/m^2).

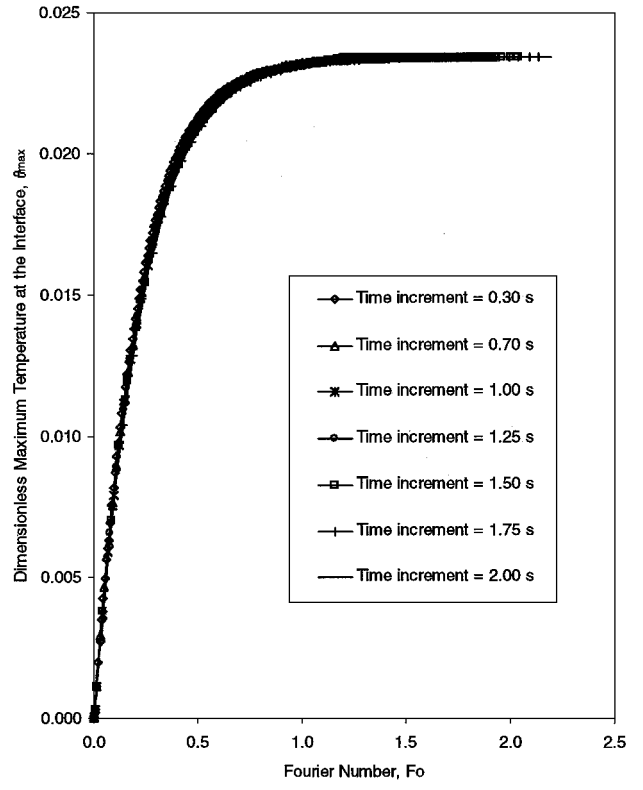

Fig. 3 Dimensionless temperature variation for different time steps ($Re = 550$, $T_j = 310$ K, $b/d_n = 2.94$, $H_n/d_n = 5$, copper plate, and $q_w = 63$ kW/m^2).

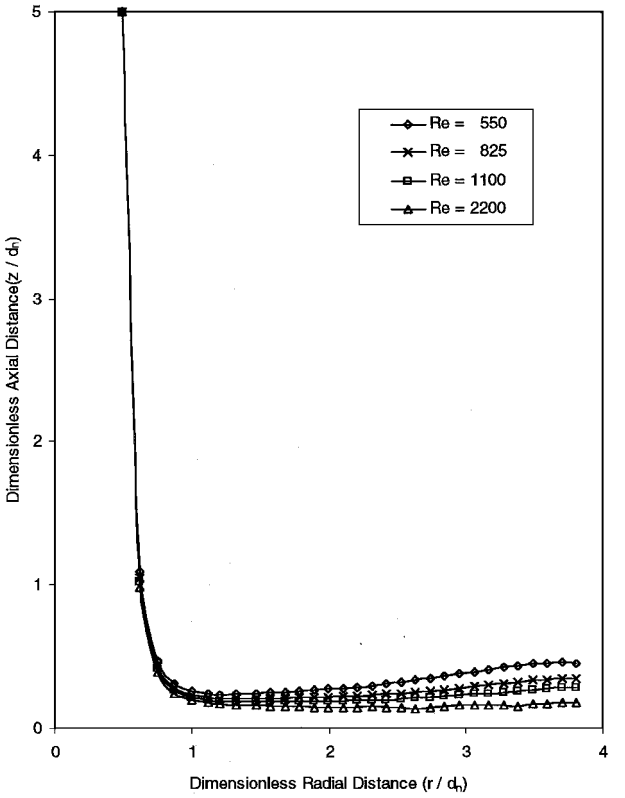

Fig. 4 Free surface height distribution for different Reynolds numbers.

To determine the number of elements for accurate numerical solution, computation was performed for several combinations of grid distribution in the horizontal and vertical directions covering the solid and fluid regions. The results for these simulations are plotted in Fig. 2. The solid–fluid interface temperature at the final steady-state condition is plotted against the downstream distance from the center of impingement. Note that the solution changes with number of elements in the horizontal and vertical directions. The solution became grid independent when the number of divisions in the horizontal direction was increased to 28, and at least 36 divisions were used in the vertical direction. There is practically no difference between results obtained with 28×36, 42×36, and 56×36 divisions. Therefore, all further computations were carried out using 42×36 elements. Computations were also performed to calculate a suitable time step to determine its sensitivity on the transient solution. Figure 3 plots the variation of maximum temperature at the interface with time for different values of time increments. Note that the simulation is not very sensitive to the size of the time step. A time increment of 1 s was selected to ensure a smooth variation.

Figure 4 presents the free-surface height distribution for different jet Reynolds numbers as the jet strikes the impinging surface. This free surface was obtained at steady-state condition. It was found that the height of the free surface did not change significantly during the transient process. Because of high Prandtl number, the thermal boundary layer is thin compared with the total height of the free surface. Therefore, significant property variation because of temperature rise with time was limited to a small region near the solid–fluid interface. The velocity in this region changed with time, but did not exert any noticeable influence on the overall height of the free surface. To validate the present fluid flow model with previous experimental and theoretical research, computation was carried out for a jet of water impinging perpendicularly at the center of a circular disk. The free-surface height distribution is shown in Fig. 5. The present results compared quite well with the experimental data of Stevens and Webb[21] and the analytical results of Watson.[22] The maximum deviation of test data from theoretical results is seen in the transition region between the stagnation zone and the

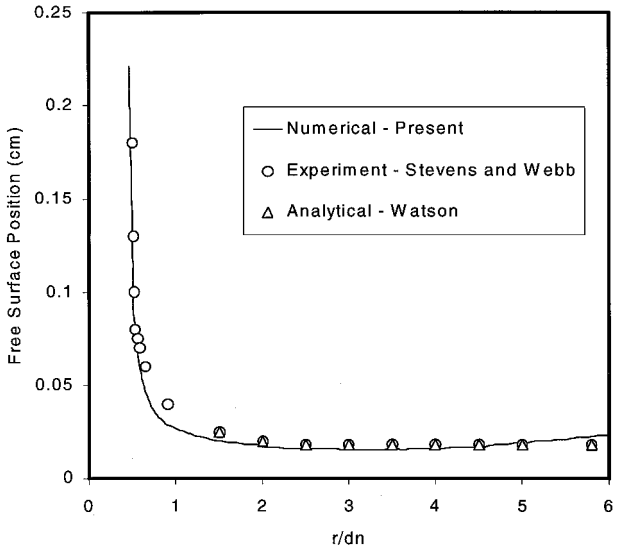

Fig. 5 Comparison of free surface height with previous investigations by Stevens and Webb[21] and Watson[22] using water as the working fluid.

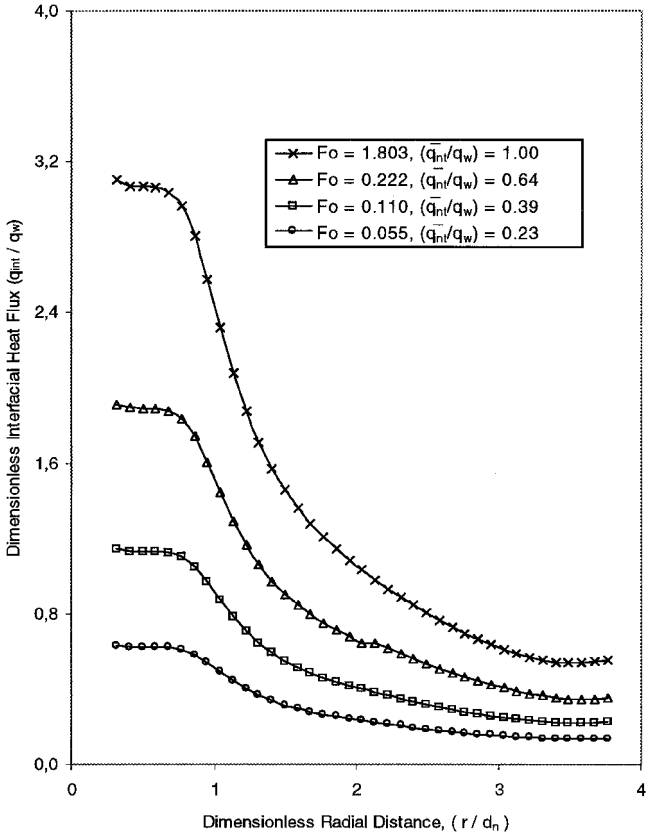

Fig. 6 Dimensionless local heat flux distribution at the interface ($Re = 550$, $T_j = 310$ K, $b/d_n = 2.94$, $H_n/d_n = 5$, copper plate, and $q_w = 63$ kW/m^2).

boundary-layer flow. The computed maximum velocity at the free surface also compared within 4% of the value reported by Stevens and Webb.[21]

A key parameter for understanding the transient heat transfer process is the local heat flux imparted to the jet at the solid–fluid interface and the total rate of heat transfer from the heat source to the coolant. These are important variables in assessing the thermal response of solid materials to the turning on of power of the heat source located on one surface and a coolant jet impinging on the opposite surface. The local heat flux distribution for different times is presented in Fig. 6. Because of initial isothermal conditions, the

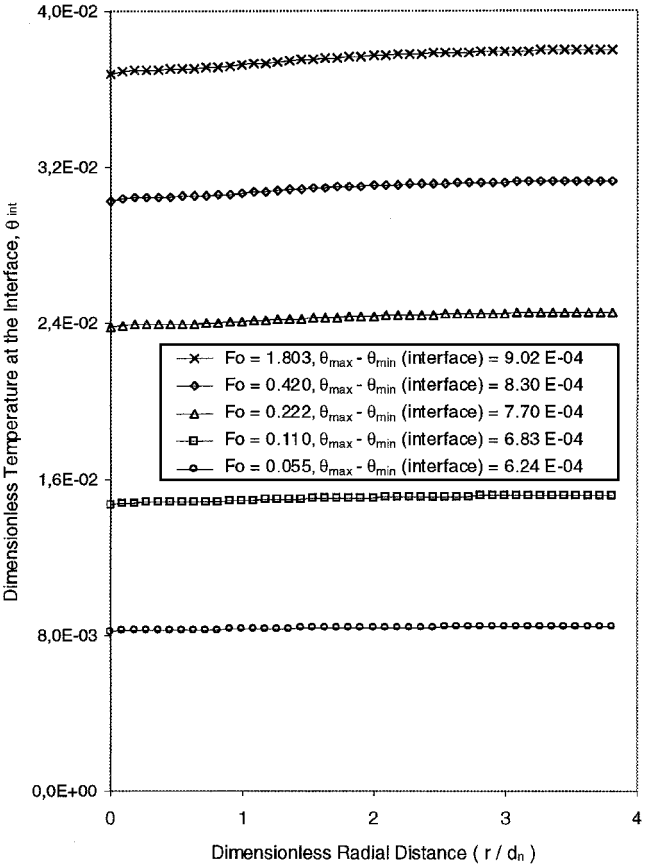

Fig. 7 Dimensionless local temperature distribution at the interface ($Re = 550$, $T_j = 310$ K, $b/d_n = 2.94$, $H_n/d_n = 5$, copper plate, and $q_w = 63$ kW/m^2).

interfacial heat flux is zero at $t = 0$. Note that heat flux at the interface increases with time. A large heat flux is seen at the stagnation region because the cold fluid at the jet strikes that location and maintains the minimum temperature at the interface. The heat transfer at that location is highest because of the constant renewal of cold fluid to carry away the heat. The heat dissipated at the heater is utilized to increase the temperature of the solid as well as the fluid. As the temperature rises with time, the thermal storage in the solid decreases and more heat proceeds to the interface and is dissipated to the liquid. The interfacial heat flux increases rapidly with time in the earlier part of the transient and more slowly as the steady-state condition is approached. For $t > 65$ s ($Fo > 1.8$), the interfacial heat flux practically reaches the steady-state distribution. Figure 6 also shows the average dimensionless interfacial heat flux at different time instants.

Figure 7 presents the interfacial temperature distribution at different times. Note that at early stages of the heat transfer process the temperature at the interface rises uniformly at all locations, resulting in a practically isothermal interface condition. This behavior is due to transient thermal storage in the fluid required to develop a thermal boundary layer starting with an isothermal initial condition. The thickness of this boundary layer increases with time and becomes significant only in the later part of the transient. The interface temperature responds accordingly. Because the leading edge of this boundary layer is located at the stagnation point and its thickness increases downstream, it can be seen that in the later part of the transient the temperature reaches a minimum at the impinging point and a maximum at the outer edge of the disk. Figure 7 presents the values for maximum-to-minimum temperature difference at the interface. As expected, the maximum-to-minimum temperature difference increases with time.

The variation of local Nusselt number with time is presented in Fig. 8. The local heat transfer coefficient increased with time in the stagnation region but decreased with time in the thin film region

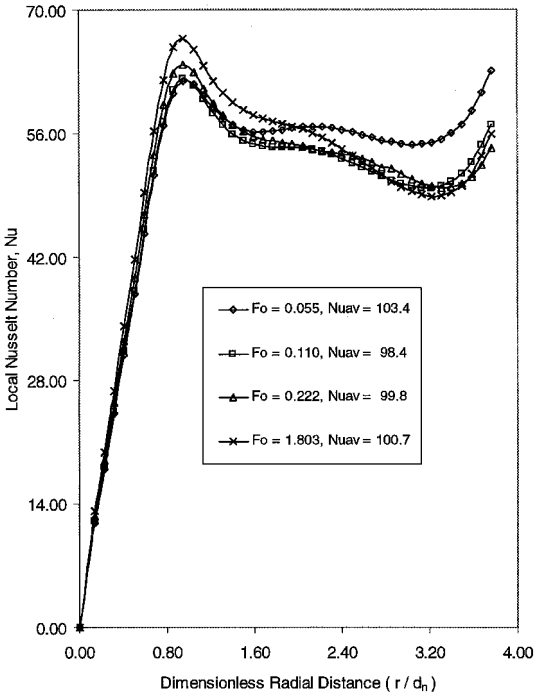

Fig. 8 Distribution of local Nusselt number ($Re = 550$, $T_j = 310$ K, $b/d_n = 2.94$, $H_n/d_n = 5$, copper plate, and $q_w = 63$ kW/m^2).

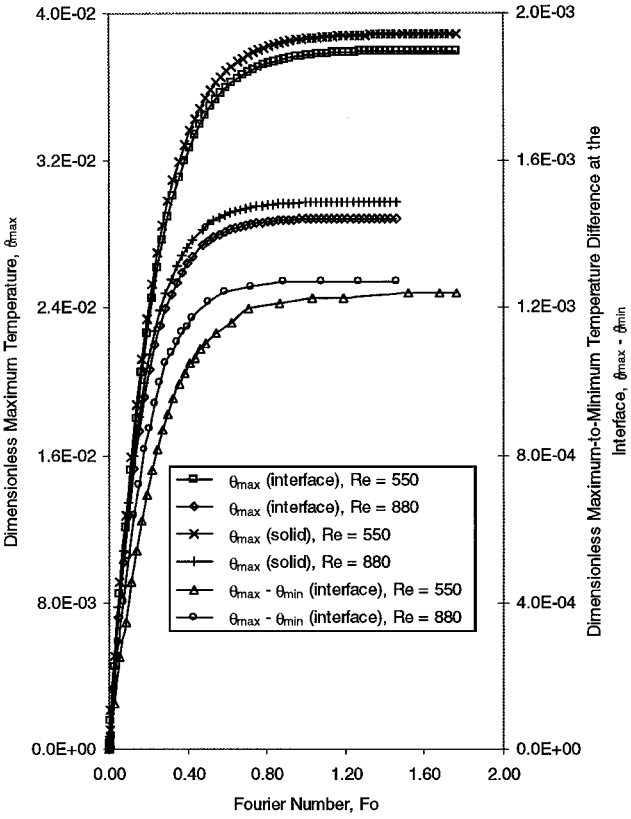

Fig. 9 Variation of dimensionless maximum temperature at the interface, inside the solid, and maximum-to-minimum temperature difference at the interface with time for different Reynolds numbers ($T_j = 310$ K, $b/d_n = 2.94$, $H_n/d_n = 5$, copper plate, and $q_w = 63$ kW/m^2).

farther downstream. Because of linear rise of length scale r used for the definition of Nusselt number, changes in heat transfer coefficient are magnified at larger distances downstream. The average heat transfer coefficient, as well as the average Nusselt number, decreases with time and reaches its respective minimum value and thereafter increases with time all of the way to the steady-state condition. This undershoot in the average heat transfer coefficient is a result of a different rate of increment for interfacial heat flux and interface temperature during the transient heating process. The local steady-state heat transfer coefficient at the stagnation region was compared with the correlation developed by Liu et al.[23] for the stagnation region heat transfer of an impinging jet including the effects of surface tension. The difference between the present computation and that predicted by the correlation was found to be around 3.9%.

The variation of maximum temperature in the solid, maximum temperature at the interface, and the maximum-to-minimum temperature difference at the interface during the transient process are presented in Fig. 9 for two different Reynolds numbers. As expected, the temperature increases with time starting from the initial isothermal condition. A rapid increment is seen at the earlier part of the transient, and it levels off as the thermal storage capacity of the solid diminishes and becomes zero at the steady-state condition. Note that the time required to reach the steady-state condition is lower at a higher Reynolds number because a higher velocity of fluid helps to enhance the convective heat transfer process. The average Nusselt number variation with time for two different Reynolds numbers is presented in Fig. 10. Note that average Nusselt number decreases with time at the early stages of the transient process and after that increases and reaches the steady-state value. Figure 11 presents the time required to reach the steady-state condition as a function of Reynolds number. The duration of the transient decreases as the Reynolds number increases. The time to reach steady state was defined as the time needed to approach 99% of the steady-state local Nusselt number over the entire solid–fluid interface.

Another important factor that controls the transient heat transfer process is the thickness of the disk. Its effect on the maximum temperature in the solid, maximum temperature at the interface, and maximum-to-minimum temperature difference at the interface can be observed in Fig. 12. As the thickness increases, the time required to reach steady state increases. This is expected because the thermal storage capacity of the disk is directly proportional to its thickness.

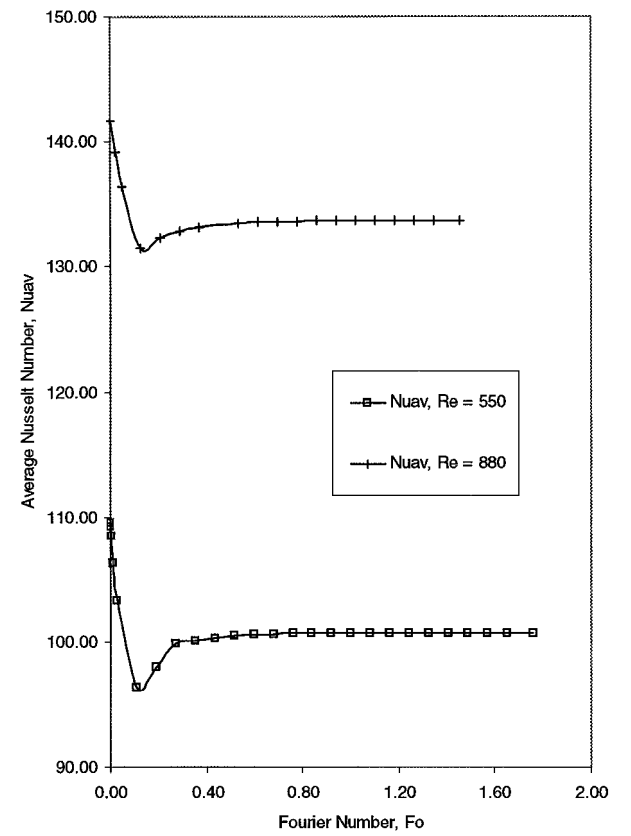

Fig. 10 Variation of average Nusselt number with time ($T_j = 310$ K, $b/d_n = 2.94$, $H_n/d_n = 5$, copper plate, and $q_w = 63$ kW/m^2).

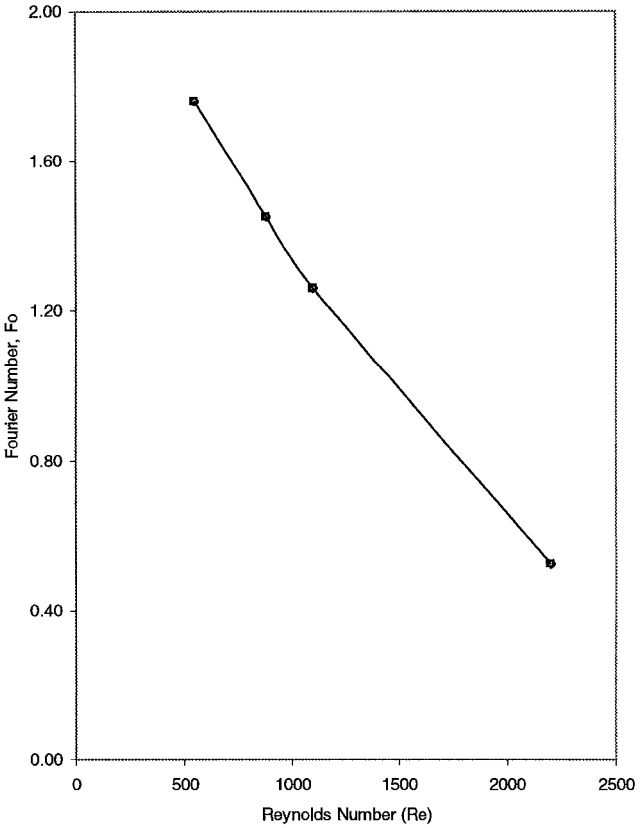

Fig. 11 Variation of time required to reach steady state with different Reynolds numbers ($T_j = 310$ K, $b/d_n = 2.94$, $H_n/d_n = 5$, copper plate, and $q_w = 63$ kW/m^2).

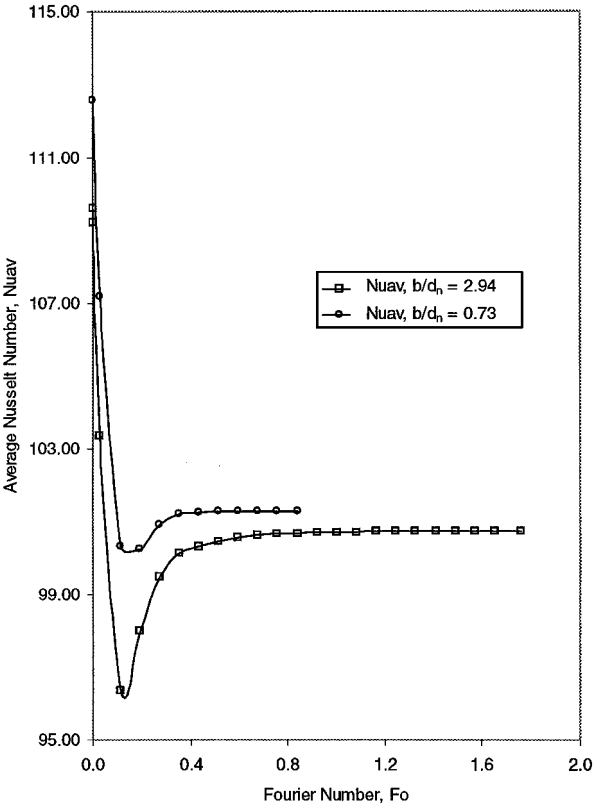

Fig. 13 Average Nusselt number variation with time for two plate thicknesses ($Re = 550$, $T_j = 310$ K, $H_n/d_n = 5$, copper plate, and $q_w = 63$ kW/m^2).

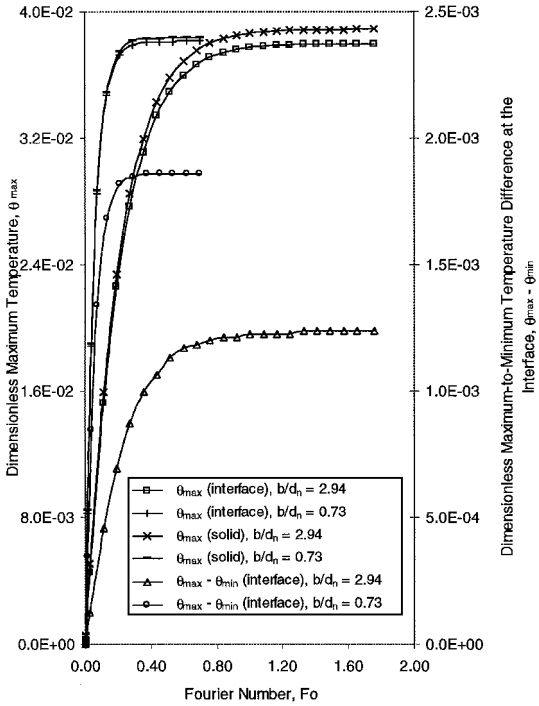

Fig. 12 Variation of dimensionless maximum temperature at the interface, inside the solid, and maximum-to-minimumtemperature difference at the interface, with time for different plate thicknesses ($Re = 550$, $T_j = 310$ K, $H_n/d_n = 5$, copper plate, and $q_w = 63$ kW/m^2).

Figure 13 presents the average Nusselt number variation with time for two different disk thicknesses. Over the entire duration of the transient process, the average Nusselt number is larger for smaller thickness. The smaller thickness presents a lower thermal resistance to heat flux and allows it to reach the interface faster.

The maximum temperature at the interface for different materials is shown in Fig. 14. Note that the material with larger thermal diffusivity reaches the steady state faster. The values of thermal diffusivity for the materials considered here at 293 K are $\alpha_{\text{diamond}} = 1.29e^{-3}$ m^2/s, $\alpha_{\text{copper}} = 1.12e^{-4}$ m^2/s, and $\alpha_{\text{constantan}} = 6.12e^{-6}$ m^2/s. As expected, the temperature changes are faster at the earlier part of the transient and only gradual as the steady state is approached. The magnitude of temperature nonuniformity at the interface at steady state is controlled by the thermal conductivity of the material. Note that constantan with $k_{\text{constantan}} = 22.7$ W/m · K has a maximum-to-minimum temperature difference of 11.1 K, whereas diamond with $k_{\text{diamond}} = 2330$ W/m · K has only a 0.2-K temperature difference at the interface. Figure 15 presents the variation of average Nusselt number with time for different materials considered in this study. In the earlier part of the transient (before the undershoot), diamond shows a larger average heat transfer coefficient compared to copper. However, after the undershoot, all of the way to the steady state, the material with lower thermal conductivity attains the higher value in the average Nusselt number. A material with lower thermal conductivity provides a higher thermal resistance within the solid. This results in a lower temperature at the solid–fluid interface when the steady-state condition is approached. This, combined with the changes in local thermal conductivity of the fluid with temperature, results in a higher Nusselt number. The time required to reach steady state for different materials and different disk thicknesses is presented in Fig. 16. As expected, as the thickness increases, the time to reach steady state increases.

Figure 17 shows the growth of the isothermal lines inside the solid at different time instants for $b = 0.005$ m ($b/d_n = 2.94$). Note that at the beginning of the transient process, the isothermal lines grow parallel to the bottom heated surface of the disk. As the time progresses,

Table 1 Comparison between experimental data of Leland and Pais[17] and numerical results obtained in present investigation[a]

Heat flux, kW/m^2	Average heat transfer coefficient, kW/m^{2}K		Percent difference
	Numerical	Experimental	
	Reynolds number 550		
63.0	4.43	3.93	11.70
126.0	4.48	4.43	1.00
189.0	4.70	4.73	1.00
252.0	4.97	4.89	1.00
	Reynolds number 800		
63.0	5.91	5.35	10.10
126.0	6.02	5.73	5.06
189.0	6.15	6.02	2.10
252.0	6.32	6.15	2.70
	Reynolds number 1100		
63.0	7.49	6.74	11.20
126.0	7.57	6.99	8.40
189.0	7.70	7.32	5.10
252.0	7.95	7.41	7.30

[a]Material, copper; $b = 0.005$ m, $Hn = 0.0085$ m.

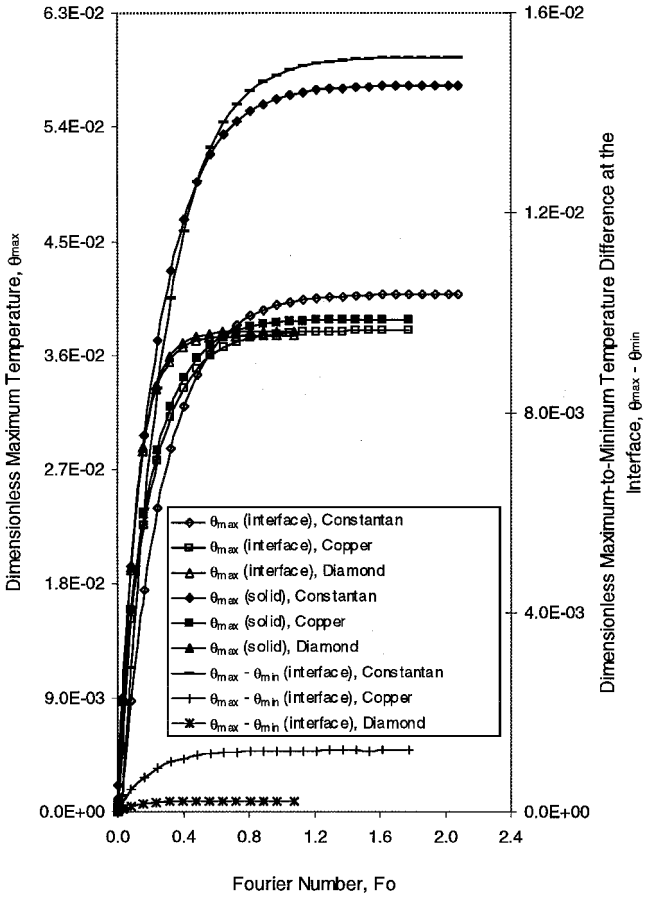

Fig. 14 Variation of dimensionless maximum temperature at the interface, inside the solid, and maximum-to-minimum temperature difference at the interface with time for different materials ($Re = 550$, $T_j = 310$ K, $b/d_n = 2.94$, $H_n/d_n = 5$, and $q_w = 63$ kW/m^2).

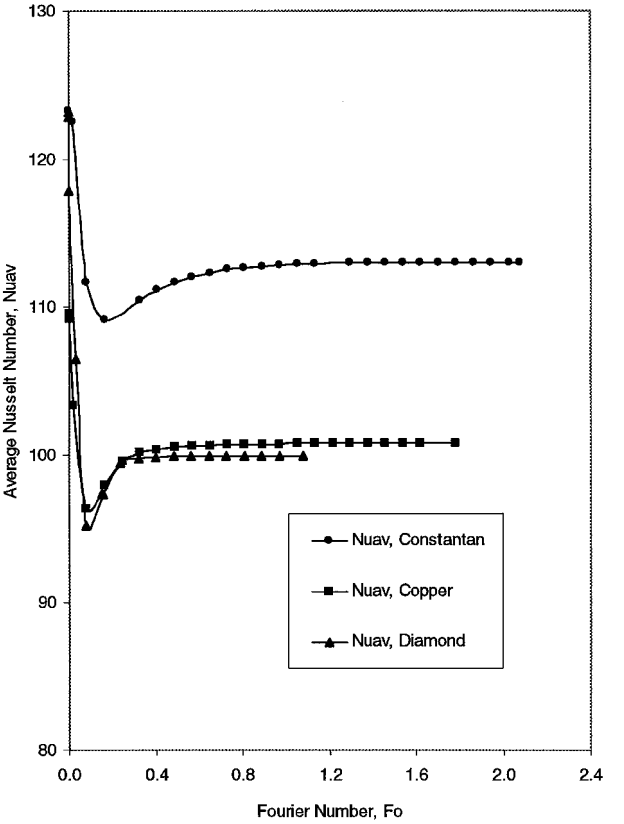

Fig. 15 Variation of average Nusselt number with time for different materials ($Re = 550$, $T_j = 310$ K, $b/d_n = 2.94$, $H_n/d_n = 5$, and $q_w = 63$ kW/m^2).

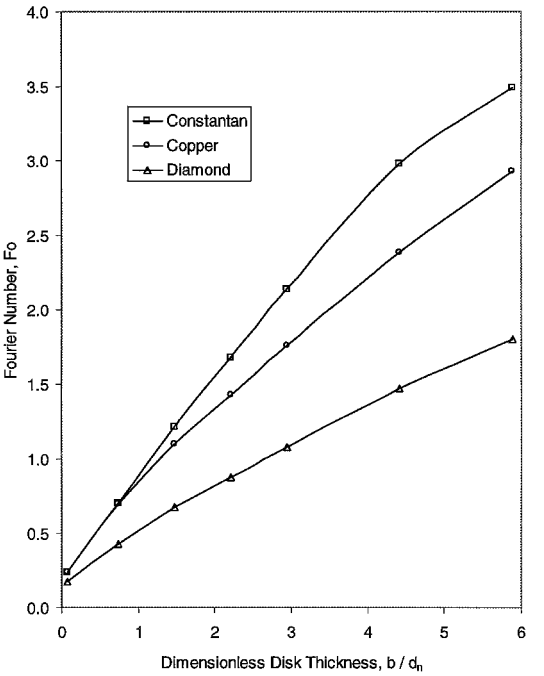

Fig. 16 Time required to reach steady state for different materials and plate thicknesses ($Re = 550$, $T_j = 310$ K, $H_n/d_n = 5$, and $q_w = 63$ kW/m^2).

the isothermal lines start moving upward like a one-dimensional heat conduction phenomenon. When the transient isothermal lines reach the area close to the interface, they start forming concentric lines around the stagnation point. As the time progresses, the effects of the heat sink are propagated down into the solid. An equilibrium is established as the steady state is approached. Note that temperature over the entire solid domain rises with time. Figure 18 plots the isothermal lines within the solid for $b = 0.0025$ m ($b/d_n = 1.47$). The behavior at the beginning of the transient process is similar to that observed in Fig. 17, but as the transient process progresses, the concentric isothermal lines around the stagnation point continue to grow and reach the bottom surface of the disk.

Because of the lack of any experimental information on the transient phenomenon, the results obtained with the present numerical model were compared with the steady-state test data acquired by Leland and Pais[17] and Womac et al.[10] The average heat transfer

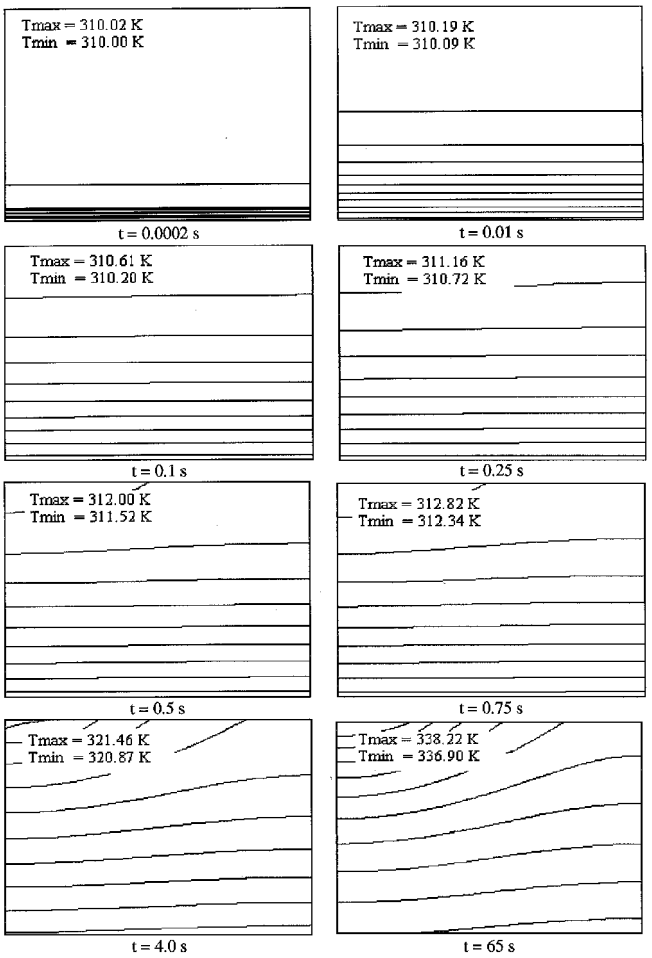

Fig. 17 Isothermal lines at different time instants for a disk of $b/d_n = 2.94$ ($Re = 550$, $T_j = 310$ K, $H_n/d_n = 5$, copper plate, and $q_w = 63$ kW/m^2).

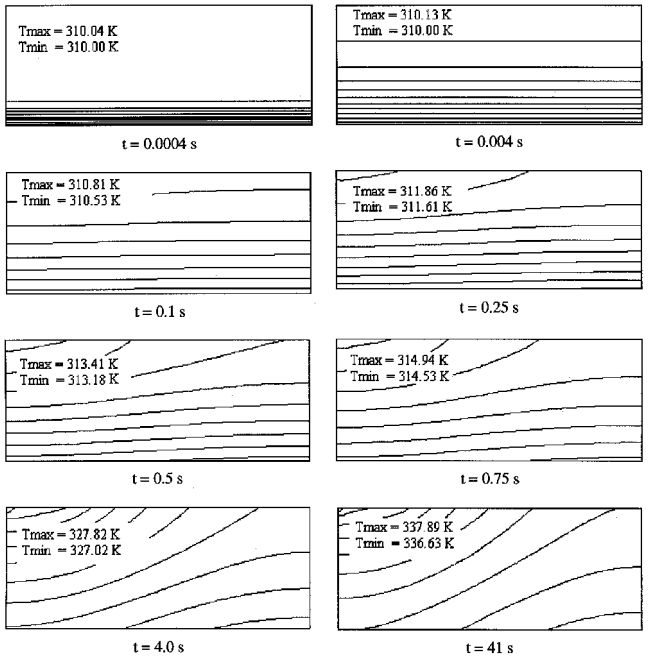

Fig. 18 Isothermal lines at different time instants for a disk of $b/d_n = 1.47$ ($Re = 550$, $T_j = 310$ K, $H_n/d_n = 5$, copper plate, and $q_w = 63$ kW/m^2).

Table 2 Comparison between present model and Womac et al.[10] model[a]

Fluid	Reynolds number	Nu_{av}, Womac et al.[10]	Nu_{av}, present study	Difference, %
FC77	1200	181.0	189.0	4.4
Water	1465	199.0	187.0	1.5

[a] $T_j = 310$ K, $b = 0.003$ m, $H_n = 0.0165$ m, copper plate, $q_w = 63$ kW/m^2.

coefficient obtained from the present numerical simulation for different combinations of Reynolds numbers and input heat flux are listed in Table 1, where they are compared with the experimental data of Leland and Pais.[17] Note that numerical predictions are within 11.7% of experimental measurements and that a better correlation of results is obtained at larger heat fluxes. The measurement errors are expected to be larger at smaller heat fluxes because of a smaller magnitude of temperature and more peripheral losses. Computationally, errors can be introduced because of roundoff and discretization. In addition, the three dimensionality of the flow due to secondary vortices in jet generation apparatus may contribute to the discrepancy between model predictions and experimental data. Considering these factors, the overall comparison with test data is quite satisfactory. A comparison between the present numerical model and the experimental data obtained by Womac et al.[10] is presented in Table 2. To carry out this comparison, numerical simulations were performed using the appropriate test fluids and heat flux conditions used in the experiment. Table 2 shows good agreement between the simulation and the experimental data, with a maximum deviation of 4.4%.

Conclusions

A number of important conclusions can be derived from the present numerical results. The local temperatures in the fluid and solid regions, as well as the heat flux at the solid–fluid interface, increase with time, but at different rates. The average heat transfer coefficient and average Nusselt number decrease with time at early stages of the transient process, after reaching a minimum; they increase to attain their steady-state values. The jet Reynolds number was found to be an important parameter controlling the transient process. The time required to reach steady-state condition decreases as the Reynolds number increases. The maximum temperature at the interface and the maximum temperature inside the solid decrease as Reynolds number increases, whereas the maximum-to-minimum temperature difference at the interface increases with Reynolds number. The time required to reach steady-state condition increases as the thickness of the disk is increased. Over the entire duration of the transient process, the average heat transfer coefficient is larger for smaller thickness. The duration of the transient is shorter for a material with higher thermal diffusivity.

References

[1] Glauert, M. B., "The Wall Jet," *Journal of Fluid Mechanics*, Vol. 1, No. 6, 1956, pp. 625–643.

[2] Metzger, D. E., Cummings, K. N., and Ruby, W. A., "Effects of Prandtl Number on Heat Transfer Characteristics of Impinging Liquid Jets," *Heat Transfer, 1974: Proceedings of the 5th International Heat Transfer Conference*, Vol. 2, Hemisphere, Washington, DC, 1974, pp. 20–24.

[3] Hrycak, P., "Heat Transfer from Round Impinging Jets to a Flat Disk," *International Journal of Heat and Mass Transfer*, Vol. 26, No. 12, 1983, pp. 1857–1865.

[4] Liu, X., and Lienhard, J. H., "Liquid Jet Impingement Heat Transfer on a Uniform Flux Surface," *Heat Transfer Phenomena in Radiation, Combustion, and Fires*, Heat Transfer Div./Vol. 106, American Society of Mechanical Engineers, Fairfield, NJ, 1989, pp. 523–530.

[5] Wang, X. S., Dagan, Z., and Jiji, L. M., "Heat Transfer Between a Circular Free Impinging Jet and a Solid Surface with Non-Uniform Wall Temperature or Wall Heat Flux—1. Solution for the Stagnation Region," *International Journal of Heat and Mass Transfer*, Vol. 32, No. 7, 1989, pp. 1351–1360.

[6] Wang, X. S., Dagan, Z., and Jiji, L. M., "Heat Transfer Between a Circular Free Impinging Jet and a Solid Surface with Non-Uniform Wall Temperature or Wall Heat Flux—2. Solution for the Boundary Layer Region," *International Journal of Heat and Mass Transfer*, Vol. 32, No. 7, 1989, pp. 1361–1371.

[7]Wang, X. S., Dagan, Z., and Jiji, L. M., "Conjugate Heat Transfer Between a Laminar Impinging Liquid Jet and a Solid Disk," *International Journal of Heat and Mass Transfer*, Vol. 32, No. 11, 1989, pp. 2189–2197.

[8]Stevens, J., and Webb, B. W., "Local Heat Transfer Coefficients Under an Axisymmetric, Single-Phase Liquid Jet," *Journal of Heat Transfer*, Vol. 113, No. 1, 1991, pp. 71–78.

[9]Liu, X., Lienhard, J. H., and Lombara, J. S., "Convective Heat Transfer by Impingement of Circular Liquid Jets," *Journal of Heat Transfer*, Vol. 113, No. 3, 1991, pp. 571–582.

[10]Womac, D. J., Ramadhyani, S., Incropera, F. P., "Correlating Equations for Impingement Cooling of Small Heat Sources with Single Circular Liquid Jets," *Journal of Heat Transfer*, Vol. 115, No. 1, 1993, pp. 106–115.

[11]Elison, B., and Webb, B. W., "Local Heat Transfer to Impinging Liquid Jets in the Initially Laminar, Transitional, and Turbulent Regimes," *International Journal of Heat and Mass Transfer*, Vol. 37, No. 8, 1994, pp. 1207–1216.

[12]Alkam, M., and Butler, P. B., "Transient Conjugate Heat Transfer Between a Laminar Stagnation Zone and a Solid Disk," *Journal of Thermophysics and Heat Transfer*, Vol. 8, No. 4, 1994, pp. 664–669.

[13]Ma, C. F., Zheng, Q., Sun, H., Wu, K., Gomi, T., and Webb, B. W., "Local Characteristics of Impingement Heat Transfer with Oblique Round Free Surface Jets of Large Prandtl Number Liquid," *International Journal of Heat and Mass Transfer*, Vol. 40, No. 10, 1997, pp. 2249–2259.

[14]Ma, C. F., Zheng, Q., Lee, S. C., and Gomi, T., "Impingement Heat Transfer and Recovery Effect with Submerged Jets of Large Prandtl Number Liquid—I. Unconfined Circular Jets," *International Journal of Heat and Mass Transfer*, Vol. 40, No. 6, 1997, pp. 1481–1490.

[15]Ma, C. F., Zhuang, Y., Lee, S. C., and Gomi, T., "Impingement Heat Transfer and Recovery Effect with Submerged Jets of Large Prandtl Number Liquid—II. Initially Laminar Confined Slot Jets," *International Journal of Heat and Mass Transfer*, Vol. 40, No. 6, 1997, pp. 1491–1500.

[16]Lee, X. C., Ma, C. F., Zheng, Q., Zhuang, Y., and Tian, Y. Q., "Numerical Study of Recovery Effect and Impingement Heat Transfer with Submerged Circular Jets of Large Prandtl Number Liquid," *International Journal of Heat and Mass Transfer*, Vol. 40, No. 11, 1997, pp. 2647–2653.

[17]Leland, J. E., and Pais, M. R., "Free Jet Impingement Heat Transfer of a High Prandtl Number Fluid Under Conditions of Highly Varying Properties," *Journal of Heat Transfer*, Vol. 121, No. 3, 1999, pp. 592–597.

[18]Burmeister, L. C., *Convective Heat Transfer*, 2nd ed., Wiley, New York, 1993, pp. 581–589.

[19]White, F. M., *Fluid Mechanics*, 4th ed., McGraw–Hill, New York, 1999, pp. 234–237.

[20]Rahman, M. M., and Faghri, A., "Analysis of Heating and Evaporation from a Liquid Film Adjacent to a Horizontal Rotating Disk," *International Journal of Heat and Mass Transfer*, Vol. 35, No. 10, 1992, pp. 2655–2664.

[21]Stevens, J., and Webb, B. W., "Measurements of the Free Surface Flow Structure Under an Impinging Free Liquid Jet," *Journal of Heat Transfer*, Vol. 114, No. 1, 1992, pp. 79–84.

[22]Watson, E. J., "The Radial Spread of a Liquid Jet Over a Horizontal Plane," *Journal of Fluid Mechanics*, Vol. 20, Pt. 3, 1964, pp. 481–499.

[23]Liu, X., Gabour, L. A., and Lienhard, J. H., "Stagnation-Point Heat Transfer During Impingement of Laminar Liquid Jets: Analysis Including Surface Tension," *Journal of Heat Transfer*, Vol. 115, No. 1, 1993, pp. 99–105.